



CHANGE OF STRUCTURAL CONDITION OF WELDED JOINTS BETWEEN HIGH-STRENGTH FINE-GRAINED AND STRUCTURAL STEELS

Jörg Hildebrand¹, Frank Werner²

Bauhaus-Universität Weimar, Marienstrasse 5, D-99423 Weimar, Germany.

E-mail: ¹ joerg.hildebrand@bauing.uni-weimar.de; ² frank.werner@bauing.uni-weimar.de

Received 1 March 2004; accepted 28 Apr 2004

Abstract. First, the production process of fine-grained structural steels was considered. The results from the thermal calculation, which is a part of the welding simulation, were compared with measurements and good concordance was achieved. A modification of the hardness was found during the analysis of the hardness curve, the so-called local hardness drop. The reason was the transformation of the structure, caused by thermal factors. The available TTA (time-temperature-austenite) and available TTT (time-temperature-transformation) diagrams do not describe this tempering process, which results in tempering structural condition by means of constituents of the martensite and bainite. The method of solution was applied to an example of a mismatch-joint and a good concordance was achieved.

Keywords: numerical simulation, high-strength fine-grained steels, MAG-welding, temperature field, hardness, tempering, local hardness drop.

1. Introduction

Today, numerical simulation offers the opportunity to observe nearly all changes during treatment and processing. By means of resolution into independent sub-processes, it makes possible to break through the complexity of the total process and look for specific solution of problems. The welding simulation consists of processes from the fields of thermodynamics, mechanics and metallurgy. Decoupled sub-processes develop according to the variously strong interaction of the three fields. The computation of the transient temperature field with transformation of structure, the stress calculation and the determination of the diffusion of gases are part of the individual processes. The list of single processes reflects the sequence of the computations, ie thermal and mechanical simulation must occur, and the diffusion of gases can be determined by the results.

Using the example of a butt weld joint, the process for the numerical computation of the temperature field and the hardness curve for an MAG-welding process is described. The transformations of structure due to thermal effects are central to the explanations. Characteristics of the simulation of the joint between structural steels and high-strength fine-grained structural steels are illustrated, and the production of the steel is described in terms of the microstructure. In addition, the computed values of temperature curve and hardness curve are compared and verified with the results of the measurement.

2. Production of fine-grained structural steels

Sheet metals with tough, ferritic-perlitic microstructure develop during traditional rolling. The microstructure is ascribed to a high rolling temperature and low resistance to deformation. For the improvement in strength and ductility properties, various procedures are used after or during rolling. Normalising, hardening and tempering and thermo-mechanical rolling are part to the processes.

For the attainment of the fine-grained structure due to normalising, the sheet metals are heated from approx. 20 to 50 °C over transformation temperature A_{c3} (final temperature of the formation of austenite when heating) after rolling and cooling afterwards. With the normalising process, the alloying elements (manganese, nickel, copper) and micro-alloying elements (niobium, vanadium, titanium) contained in the steel have an effect on the structure. With the cooling, a fine grained matrix is developed and the ductility is increased by a delay γ - α -transformation with nickel. The formation of mixed crystals from manganese and nickel with the iron also improves the ductility properties of the steel. Micro-alloying elements and copper cause a precipitation hardening, which is reflected by an increase in the strength properties. Steels manufactured using the normalising process attain a yield strength between 235 and 500 N/mm² and have a structure of polygonal ferrite and pearlite.

After rolling, the sheet metal goes through two heating processes, hardening and tempering. The first step, hardening, includes a heating of sheet metals over the A_{c3} -temperature and a subsequent fast cooling with a speed of 40–50 K/s. The quenched structure is developed from martensite and bainite with a disproportionately high carbon content. In the second step, the sheet metals are heated to the transformation temperature A_{c1} (starting temperature for the formation of austenite when heating). The process is referred to as tempering. The existing structure of martensite and bainite thereby separates finely distributed carbide. At the end of the two processes, the sheet metals have tempered carbon-poor martensite and tempered fine-grained bainite.

The alloying elements (manganese, molybdenum, chrome, nickel) and micro-alloying elements (vanadium, boron, titanium) change the transformation temperatures of the steel and decrease the critical cooling rates for the formation of martensite and bainite. The favoured structure in the sheet metal can be produced with economically favourable and technically possible cooling rates. The existence of martensite and bainite is a prerequisite for the production of high-strength structural steels. The developed fine-grained structure contributes to an increase in ductility without loss of strength. Fine-grained structural steels with a yield strength between 460 and 960 N/m² could be manufactured by hardening and tempering. The steels also have good ductility properties.

Using thermo-mechanical rolling, a new delivery condition is developed involving a deliberate control of temperature, deformation and time during rolling. The sequence is divided into three phases. During the first process, the pre-rolling phase, the steel slabs are rolled to an intermediate thickness with a fine-grained and regularly developed austenite structure. In the second process, the weaving phase, the steel slabs are cooled without rolling. The new grain formation of the structure is prevented by separating compounds with the micro-alloying elements (carbonitrid). A further refinement of the austenite grain is caused during the final rolling, dependent on temperature and deformation. In the sheet metals, a ferritic and a lamellar pearlitic structure is developed from a modified austenite structure after a final rolling and a slow cooling. The quenching with water (15–20 K/s) causes a modification from austenite to bainite. The result is an increase in strength. Ductility is achieved as a result of the fine-grained structure. Subsequent tempering is necessary for sheet metals with high-strength requirement. For this purpose, precipitation hardening is used during the tempering. The thermo-mechanically rolled steels have a high weldability as a result of the low-alloying element concentration. The sheet metals are suitable for welding with high cooling rates. A schematic overview of the three manufacturing processes and the yield strength of fine-grained structural steels can be seen in Fig 1.

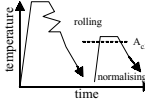
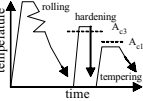
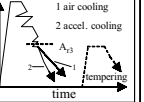
Process	Normalising	Hardening and tempering	Thermo mechanical rolling
Treatment			
Texture	polygonal ferrite, pearlite	tempered martensite, tempered bainite	stretched/spicular ferrite, pearlite bainite
Steelgrade / application	example: structural steel, shipbuilding steel	example: high-strength steel	example: structural steel, shipbuilding steel
Yield strength [MPa]	235–500	460–960	235–690

Fig 1. Schematic overview of the manufacturing processes of fine-grained structural steels after [1]

From the viewpoint of the structural condition, steel can be represented as an inhomogeneously composed material dependent on the manufacturing process. Each constituent of the microstructure (ferrite, pearlite, martensite and bainite) has different mechanical and thermal properties, which can be used to determine the steel composition. For this purpose, one needs to know the manufacturing process used and the data available in the literature for the yield strength of the constituents of the microstructure. The result for the steel is shown in Table 1.

Table 1. Percentage composition of the microstructure dependent on the steel

Steel	Structure	Ferrite [%]	Pearlite [%]	Bainite [%]	Martensite [%]
S355NL/ML	80	20	0	0	
S460NL/ML	10	90	0	0	
S690QL	0	0	86	14	
S960QL	0	0	25	75	
S1100QL	0	0	0	100	

The data in Table 1 represent the starting point for the description of the steel on the basis of the microstructure characteristics, using the numerical computation of the temperature field and the residual stresses. The effects of the manufacturing on the structural condition are included. Observation of the production of fine-grained structural steels is necessary for a characterisation of the available initial state.

3. Welding simulation

Numerical welding simulations provide an opportunity to analyse modifications during the welding process more exactly. Analysis of the welding is complicated by the complex physical interactions of processes from the fields of thermodynamics, mechanics and metallurgy.

A decoupling of the large model into several simple models with reduced computation expenditure can be accomplished by knowledge and consideration of the variously strong and interdependent influences between the sub-processes.

The transient temperature field directly affects the structural condition. In contrast, the diffusion of gases has only a slight effect on temperature distribution. Further examples are found in [2]. In the partition often used in the literature, the large model is divided into models for the computation of the temperature field with transformation of the structure, for mechanical computation and for the determination of the diffusion of gases. Further presentations are limited to thermal simulation and transformation of the structure. The hardness at the welded joint is calculated numerically, based on the results of the thermal computation.

3.1. Temperature field

The phase- and temperature-dependent values of the material were used for enthalpy and heat conductivity in the thermal simulation of the transient temperature field and based on the results from Chapter 2. The material data used for the individual constituents of the micro-structure is based on an evaluation of the literature and can be seen in Figs 2, 3.

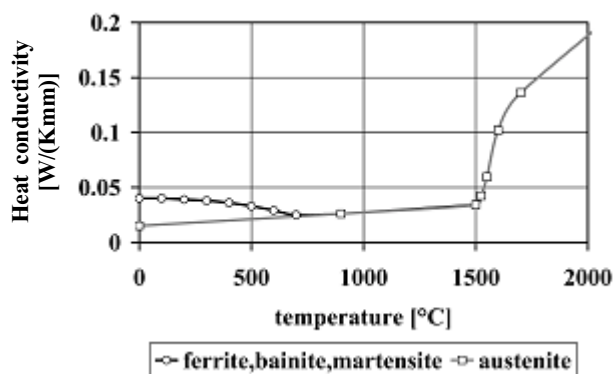


Fig 2. Heat conductivity

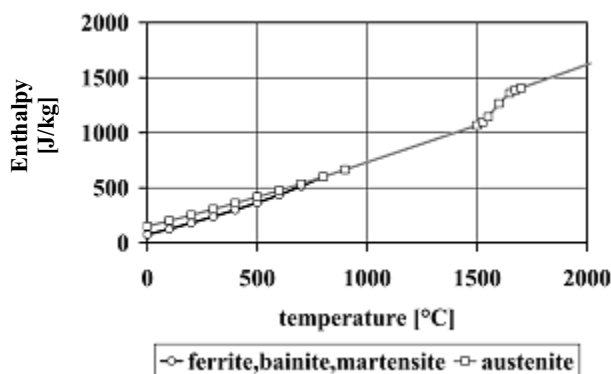


Fig 3. Enthalpy

During the heating, α -iron (ferrite, martensite, bainite, perlite) is transformed into γ -iron (austenite) under volume modification. The process takes place in a temperature range between ~ 700 °C and 850 °C, dependent on the chemical composition. The transformation of the structure during the heating process can be illustrated by a time-temperature diagram for continuous heating (TTA diagram). A time-temperature diagram for continuous heating for the steel S355N is given in [3]. Further time-temperature diagrams for continuous heating for other fine-grained structural steels could not be found in the literature. The transformation of γ -iron into α -iron is started with the cooling of the steel in the lower temperature range. The transformation of structure is significant for the formation of residual stresses. Some of the chemical-composition-dependent TTT diagrams can be found in [4], for example, structural steels, high-strength and corrosion-resistant steels, weldability structural steels and MAG weld metal. The diagrams have been developed for a welding temperature cycle. The TTT diagrams for new high-strength, quenched and tempered, fine-grained structural steels are given in [5] for S960Q and in [6] for S1100QL.

The parent metals, as well as the filler metals, are similarly transformed during MAG-welding. Substantial differences were determined by comparison with the chemical compositions between the measured values from the experiments and the values documented in [4]. However, the existing TTT diagrams in [4] are unsuitable for application to the modern filler metal in the numerical computation. Therefore, the transformation of structure is described by an empirical formulation, which is stated for the first time in [7] and has been further developed since. By means of the aforementioned formulation, the percentage composition of any low-alloy filler metal can be determined without realisation of tests, and TTT diagrams can be developed. An example of a TTT diagram for the filler metal “Union MoNi” can be seen in Fig 4. The continuous transformation of the structure can be considered during the simulation by means of the Leblond kinetic model within the FE-program SYSWELD [8].

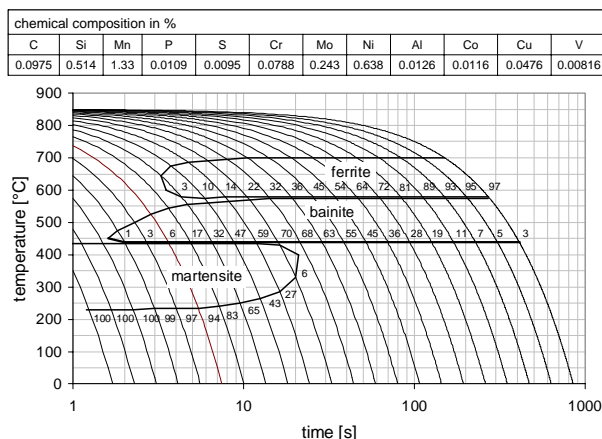


Fig 4. Welding TTT diagram for welding consumables “Union MoNi”

A cause of the transformation in the material is locally active heat input during welding. Different models for heat sources, as well as for the formulation in the numerical computation, exist in the literature. Goldak presents a normal distributed heat source for TIG- and MIG-welding methods in [9]. A further development is a normal source in the form of ellipsoids in [10], which is characterised by a closed representation form. The factors f_r and f_r , the so-called heat transfer coefficients, from the formulation in [9] are omitted [10]. This is represented by simplification during adjustment to conditions. The change in the formulation of the heat source is limited by the geometrical dimension a , b , c . The dimension of the heat source depends on the respective welding process. An adjustment of the heat source to the ambient conditions is important. The heat is transferred to the environment separately from the application of energy during welding. The heat emission consists of radiation and convection. The radiation is described by the Stefan-Boltzmann law. The part of the radiant heat is greater in relation to the heat transfer by convection at high temperatures. The heat flow volumes are dependent on the heat transmission coefficient in the case of convection. Data for convection can be found in the literature. For further details, refer to [11] and [12].

After description of the necessary data of the thermal simulation, the temperature field is simulated using the example of a butt weld. The used material data are shown in Table 2. The structure of the three-layer butt weld can be seen in the macrograph and it was considered in the FE-model for the joint of the 10-mm-thick sheet metals.

Table 2. Material data used

Parent metal 1	Parent metal 2	Filler metal
S355	S960Q	G Mn3Ni1Mo EN 12534 (Union MoNi)

For the calibration of the temperature field computation, as well as for the validation of the assumptions and the simplifications, the temperature field during welding was measured by thermocouples of the type NiCr-Ni. A mobile measurement technique, developed at the beginning of the project, was used. The results of the measurements and the simulations are shown in Fig 5. The comparison shows a high degree of concordance between computed and measured temperature. The max temperature difference is 12 K.

The easily identifiable expansion of the melting bath in the macrograph picture and maximum expansions of the molten pool, which are described by the 1500 °C limit in the simulation, were compared for each weld layer and thus for further validation of the simulation. A high degree of concordance was also found in the results here.

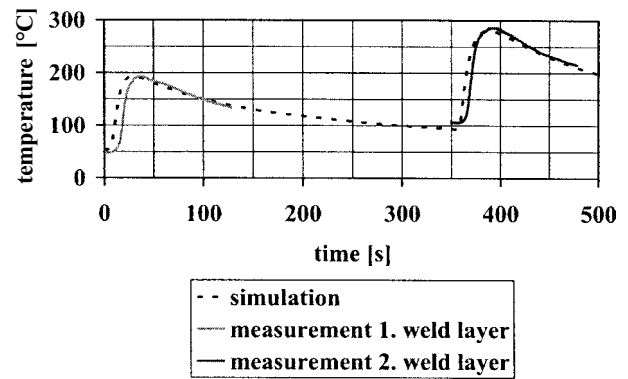


Fig 5. Comparison between measurement and simulation

The properties in the heat-affected zone (HAZ) of fusion welding joints are affected by welding process conditions and by chemical composition. The technical term, welding conditions, indicates welding methods, welding parameters, work temperature and form of weld. A central term, the cooling time $t_{8/5}$, was introduced for evaluating the welding process in practice. This value marks the length of time for passing through the 800 °C limit up to the 500 °C limit at one location during cooling. The significant transformation processes in the steel take place in this temperature range. The cooling time and the properties in the HAZ are directly linked. Simple formulations have been developed for the prediction of cooling time for practical application. A differentiation between two- and three-dimensional heat conduction is made in [13]. The equation for two-dimensional heat conduction is:

$$t_{8/5} = (4300 - 4,3T_0)10^5 \frac{Q^2}{d^2} \left[\left(\frac{1}{500 - T_0} \right)^2 - \left(\frac{1}{800 - T_0} \right)^2 \right] F_2 \quad (1)$$

and the cooling time for three-dimensional heat conduction results from the following mathematical context:

$$t_{8/5} = (6700 - 5T_0)Q \left[\left(\frac{1}{500 - T_0} \right) - \left(\frac{1}{800 - T_0} \right) \right] F_3 \quad (2)$$

The reduced heat input per unit length of weld Q [kJ/mm], the preheat- or interpass-temperature T_0 [°C], the weld factor F [-] and the sheet metal thickness d [mm] are required for computing the cooling time $t_{8/5}$ in s. The cooling time can be determined by means of the equation (1) and (2) for each weld layer during the three-layer welded joint with the material data in Table 2 and the welding parameters in Table 3.

The values for two-dimensional (2d) and three-dimensional (3d) heat conduction are compared to determine the specifying cooling times for each weld layer from Table 4.

Table 3. Welding parameters

Weld layer	Welding position	Welding current	Welding strain	Welding speed
–	Pos	A	V	mm/s
1	PA	270	31,8	10,38
2	PA	275	31,8	8,33
3	PA	276	31,6	8,33

Table 4. Cooling time

Weld layer	Cooling time	
	[s]	
–	2d	3d
1	6,58	3,95
2	11,27	5,22
3	10,84	5,36

The greater numerical value is the determining factor. Variations of up to 10 % are possible between measured and computed values for the cooling time with simple butt weld joints. Error is greatly increased in the case of complicated geometry. Variations of up to 100 % are possible. The computed values with equations (1) and (2) refer to the point of the weld characterised in Fig 6. A cooling time is ascertainable for one point with another geometrical situation with the equations. The cooling time for each weld can be seen separately in Fig 6. The change of the cooling time shows up from the ranges of the weld over the HAZ to the unaffected

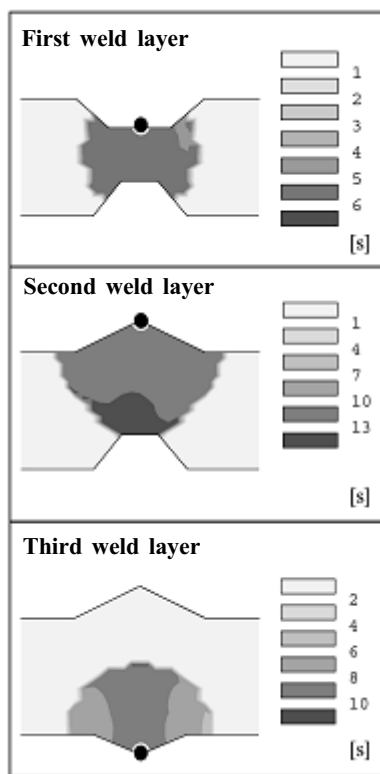


Fig 6. Cooling time for each weld layer with marked point

parent metal in the weld layer. The variations are of a maximum of 10 % between the cooling times after the equations (1), (2) and from the FE-simulation for each weld layer. A high degree of concordance was also found in the results here.

The numerically computed temperature field was compared with the temperature curve at the selected point. In addition, the geometry of the melting bath from the macrograph picture was compared with the expansion of the maximum temperature limit by 1500 °C from the FE-simulation. Additionally the cooling times were considered between the practice-relevant equations after [13] and the FE-computation. High degrees of concordance were obtained in all three comparisons. It can thus be shown that the temperature field of the simulation calculation is in a high concordance with the real welding.

3.2. Microstructure

It is well-known from Chapter 1 that steel is made up of the individual constituents of the microstructure (ferrite, pearlite, bainite and martensite) after the production process. The mechanical and thermal properties of steel are determined by the combination of the properties of the microstructure. Modifications in the constituents of the microstructure are found in the HAZ during the processing and the treatment of the steel by welding processes. The main reason for the change is seen in the existence of the temperature field during welding. This special kind of thermal treatment of steel with the strong temperature gradients over the material is illustrated by the TTA and TTT diagrams. Diagrams are available for consideration using the numerical simulation.

Fig 7 shows a steel S355 on the left-hand side and a steel S960Q on the right-hand side. The percentage composition for the two steels, specified in Table 1, was

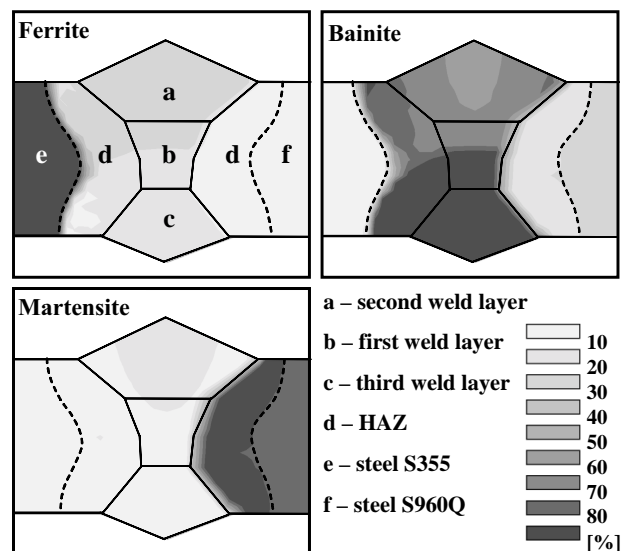


Fig 7. Percentage distribution of constituents of microstructure after third weld layer

considered using the numerical simulation. The initial composition of steel S960Q is characterised by ~75 % martensite and ~25 % bainite. The steel S355 consists of 100 % ferrite. At the beginning of the welding, the weld metal consists of 100 % austenite and is transformed into ferrite, bainite and martensite during the cooling process.

The effects of the temperature field on the three constituents of the microstructure within the area of the weld and the HAZ can be seen in Fig 7. The different constituents of the microstructure in the separate areas after welding exert an influence on the properties of the mismatch-joint. These include, for example, the residual stress and the fatigue behaviour of this joint. The high-strength steels S960Q generate far more martensite in the region from weld to parent metal in relation to the composition in the initial state. In the range d of the high-strength steels S960Q, a darker colour can be recognized in Fig 7. The so-called microstructure notch exists in addition to the existing geometry notch. The combinations of material and geometrical properties have an unfavourable effect on the fatigue behaviour in the range weld – parent metal with mismatch-joints. Ongoing investigations have shown this.

4. Calculation of hardness

During the evaluation of experimental results, it was stated that a drop in the hardness curve occurs after the hardness peak in high-strength fine-grained structural steel. The minimum hardness value in the so-called local hardness drop is around 53 HV5 for S690QL and around 70 HV5 for S960QL with the values of the unaffected parent metal. A local drop was not observed around 50 HV5 of the hardness in the subsequent range of the HAZ with steels with lower yield stress (S355 and S460). The hardness curves for two welds are represented in Fig 8 for cruciform joints at the top side of the weld.

In the combination of S355M with S690QL, the sheet metal with the lower yield strength is set on the sheet metal with a higher yield strength. An influence on the structure can be excluded within the range of the groove by joint preparation with the sheet metal S690QL. But the low-strength sheet metal runs through continuously in the case of the combination S960QL with S460M. A joint preparation with thermal effect and consequent structural changes in the high-strength sheet metal cannot be detected in the hardness curve.

The steels S690QL and S960QL both come from the group of fine-grained structural steels with hardening and tempering. The initial structure after production consists of martensite and bainite. Further temperatures up to a maximum of 700 °C predominate within the range of the reduced hardness during the weld. Therefore, a transformation to austenite does not occur within the sub-critical heated-up range. The change in speed for heat-

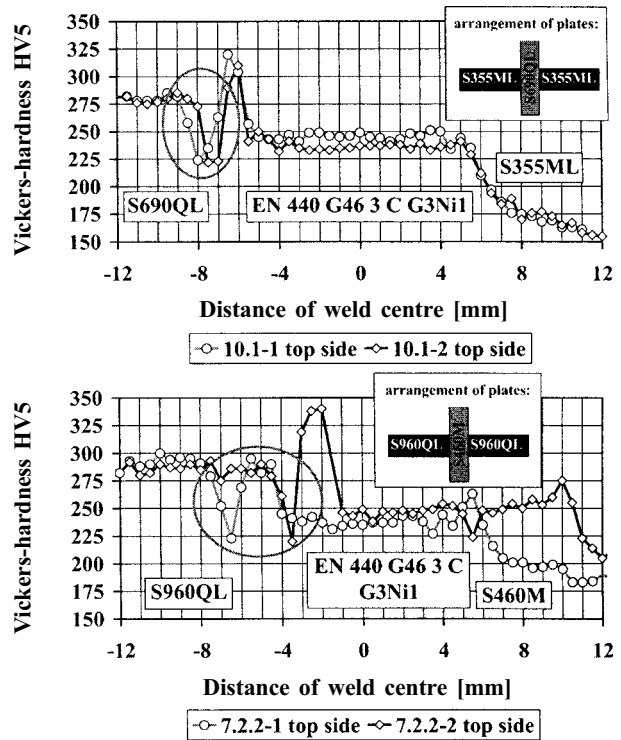


Fig 8. Hardness curves of cruciform joints

ing and cooling for two points within the range of the local hardness drop can be seen in Fig 9. The maximum temperature for a point 7,8 mm away from the centre of the weld is 675 °C.

Similar initial conditions are the case with multiple layer welding. The tempering zone is defined between the Ac1-temperature (~700 °C) and the martensite starting temperature. In this zone, a relaxation of the structure (recrystallisation) occurs by means of the tempering processes and leads to a reduction in strength. The descriptions found in the literature for the tempering processes refer to the thermal treatments of steel segments in hourly stages. On the other hand, the heat works only briefly during the weld, as Fig 9 shows. The available thermal treatment approaches cannot be used for condi-

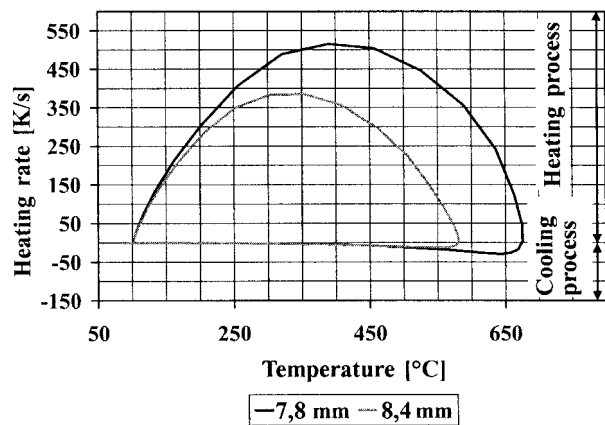


Fig 9. Heating and cooling rate during MAG-welding

tions during welding. The present approach considers a modification of the numerical simulation in the structure. A functional connection was sought between heating rate, temperature and change in the constituents of the microstructure during the tempering, limited to the constituents of the microstructure martensite and bainite. Two processes exist during the heating of steel in the numerical simulation. This behaviour refers to the conversion of the initial structure into austenite. The other relationship describes the change of martensite or bainite into tempered martensite or tempered bainite.

The interdependence between temperature, heating rate and transformed microstructure is represented in Fig 10.

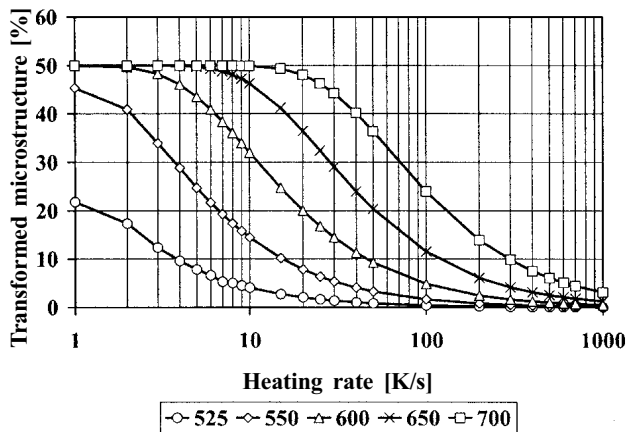


Fig 10. Transformed microstructure dependent on heating rate and temperature

The diagram can be understood as follows: 50 % of the initial structure transforms into tempered structure during a heating rate from 1 K/s to 700 °C; 50 % of both the martensite and the bainite changes into tempered structure; if the initial structure of 100 % martensite is heated with constant 20 K/s to 600 °C, then a ratio of 20 % tempered to 80 % unchanged martensite is in the steel at the end of the cooling process; a maximum upper limit for the transformed structure is determined at of 50 % of the initial structure and occurs at high temperatures and slow heating rates. If the temperatures are developed over the A_{c1} -temperature with a weld layer, what has so far been a tempered structure disassembles itself linearly up to the A_{c3} -temperature, and austenite is created. The temperature and the speed change simultaneously with the heating process during the welding. This is seen in Fig 9. The kinetic model of Lebond is used for the application in the FE-program SYSWELD. This model for the transformation behaviour has already been used for the conversion of the TTA and TTT diagrams.

The effects of tempering can be clearly seen in Fig 11. A zone of up to 30 % tempered structure is cre-

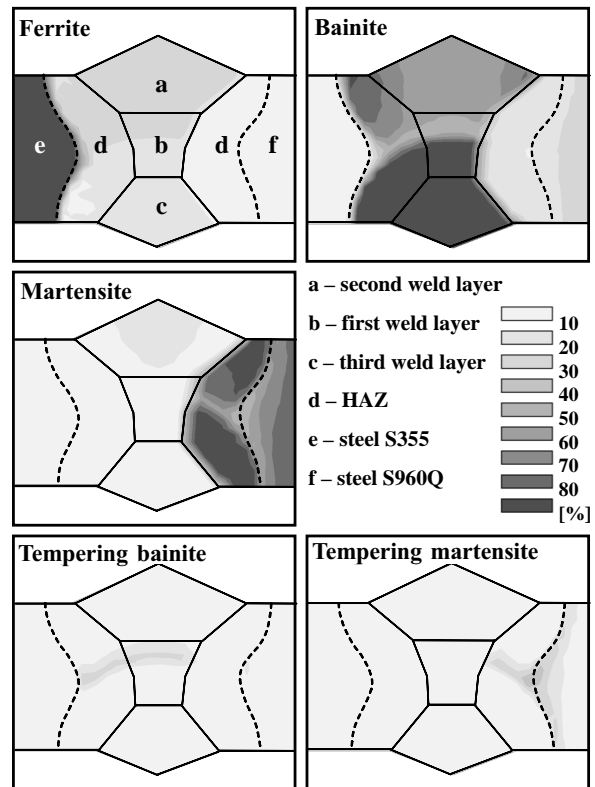


Fig 11. Percentage distribution of constituents of the microstructure after third weld layer with regard to tempering effect

ated over the third and final weld of the butt weld joint. A line of tempered martensite appears in the high-strength fine-grained structural steel from the upper surface to the base with the parent metal on the edge of the HAZ. In addition, a part of the bainite, resulting from the preceding weld layers, is transformed both in the weld and in the parent metal of the low-strength fine-grained structural steel. The tempering of the structure near the HAZ is considered in the numerical simulation.

The hardness of the transformed structural condition is calculated. Different empirical models exist in the literature for the determination of hardness. The formulations for individual constituents of the micro-structure (ferrite, pearlite, bainite and martensite) are deduced using systematic investigations and by means of the regression analysis of a large number of results. The values of hardness depend on chemical composition. The effects of the change in temperature are taken into account in the formulations through the cooling speed of 700 °C or the cooling time $t_{8/5}$. The consideration of portions of the residual austenite is not relevant from a carbon content of 0,50 %. The low-alloy structural steels have a maximum carbon content of 0,20 %.

The following three equations are available for the numerical determination of the hardness values in the FE-program SYSWELD:

hardness of martensite

$$HV_M = 127 + 949C + 27Si + 11Mn + 8Ni + 16Cr + 21 \log \left(\frac{d\theta}{dt} \right), \quad (3)$$

hardness of bainite

$$HV_B = -323 + 185C + 330Si + 153Mn + 65Ni + 144Cr + 191Mo + (89 + 53C - 55Si - 22Mn - 10Ni - 20Cr - 33Mo) \log \left(\frac{d\theta}{dt} \right), \quad (4)$$

hardness of ferrite

$$HV_F = 62 + 223C + 15Si + 30Mn + 21Ni + 23Cr + 19Mo + 260V. \quad (5)$$

The equations (3) to (5) are based on the investigations of R. Blondeau et al [14] and [15]. The hardness of pearlite is computed using the formulation for ferrite. The total hardness of the steel is computed dependent on the percentage portions of the constituents of the microstructure. For the tempered structure, the hardness of ferrite is used. The linear mixture rule for the determination of hardness, available in the FE-program SYSWELD, is as follows:

$$HV = (y_{ferrite} + y_{pearlite} + y_{temp.martensite} + y_{temp.bainite}) \cdot HV_F + y_{bainite} \cdot HV_B + y_{martensite} \cdot HV_M.$$

Applied to the example, the hardness values are calculated for the second weld layer and can be seen in Fig 12. The hardness curve with regard to the tempering effect adapts better to the results of measurement. The dropping in hardness can be reproduced within a range of 6 – 8 mm adjacent to the centre of the weld in the high-strength parent metal. The maximum hardness difference with tempering is 17 HV between measurement and calculation. A peak develops in the numerical simulation at the edge of the weld at a value of 400 HV in the hardness curve without regard to tempering. The

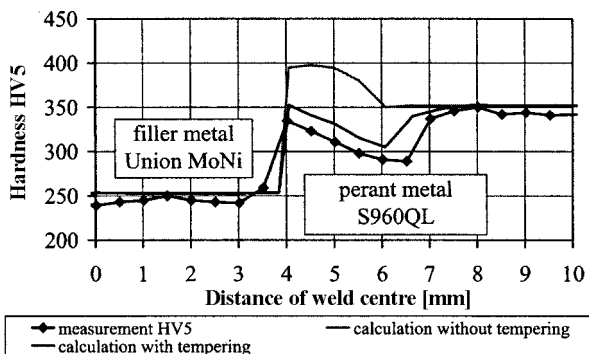


Fig 12. Comparison of hardness curves after the second welding

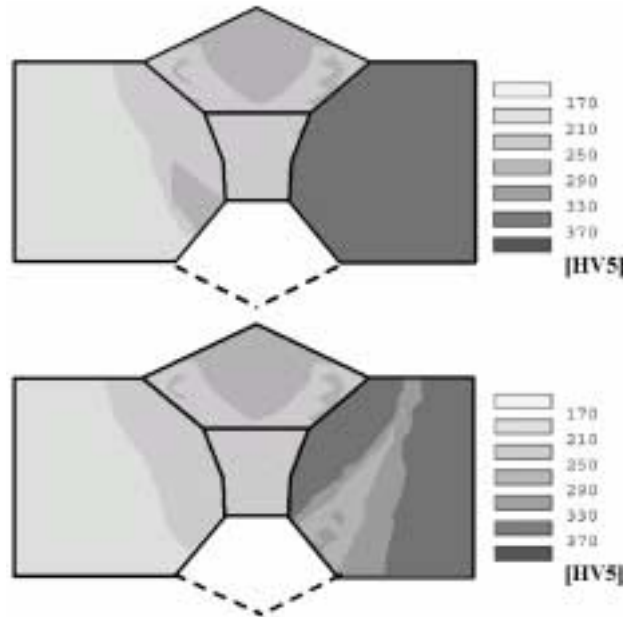


Fig 13. Hardness distribution after the second weld layer without regard to the tempering effect (above) and with regard to the tempering effect (down)

hardness value is more than 50 HV higher in relation to the measurement. The hardness over the total cross-section after the second weld layer with and without regard to tempering can be seen in Fig 13.

The peak drops in the lower part of the missing third weld in low-strength steel. The portions of martensite and bainite are lower in this area after the first welding in relation to the initial situation in high-strength steel. The effects of tempering on the structure, and thus on the hardness, can be recognised in the right-hand section of the butt weld joint. An improvement in the results can be produced through the expanded formulation in the numerical simulation.

5. Summary

After the introduction, the second chapter deals with the production of fine-grained structural steels and the associated structural conditions in steel. Steel is an inhomogeneous material in terms of its microstructure. The material data for the thermal calculation in the welding simulation is described in the third chapter. The results of the simulation are compared with measurements by means of an example. The FE- program SYSWELD is used for the calculation. A high degree of concordance is obtained in temperature curves, in the expansion of the molten pool and in the cooling time for the three weld layers. The transformations of the structure, which are described by TTA- and TTT-diagrams, are discussed in chapter 3.2. An extension to the consideration of the tempering of martensite and bainite is presented in chapter 4 and converted into the FE-program SYSWELD using the Leblond kinetic model. The calculation of hard-

ness is a further main area in chapter 4. A high degree of concordance between measurement and numerical calculation is achieved using the example. The results of the hardness curves show that an extension of the transformation behaviour is necessary in the case of steels with martensite or bainite sections. A comprehensive view of the level of the microstructure from the production to the end of the treatment process demonstrates the causes and solutions observed during the welding process.

6. Acknowledgement

The authors would like to thank the “Thüringer Ministerium für Wissenschaft, Forschung und Kunst (TMWFK)” for its financial support. Schachtbau Nordhausen GmbH are also to be thanked for making the welded samples. IFW Jena gGmbH carried out the hardness tests and the measurements of the chemical compositions. Dr.-Ing. H. Heinemann at IFW Jena gGmbH, Dipl.-Ing. E. Kröner and Dipl.-Ing. B. Senk at Schachtbau Nordhausen GmbH are to be thanked for their support of the project.

References

1. Kolleck, M. Investigations of materials by welding of microalloyed high-strength fine-grained structural steels. Doctor thesis. Clausthal Technical University, 1996. 151 p. (in German).
2. Wohlfahrt, H. Simulation of processes in the weld pool with the laser welding to the prediction of weld shape, microstructure, distortion and residual stresses. Research report Aif 11.583 A/B, Brunswick, 2002. 135 p. (in German).
3. Degenkolbe, J.; Hougardy, H. P.; Uwer, D. Bulletin 381 „Welding of unalloyed and low-alloy structural steels. Steel Information Centre, Düsseldorf, 1999. 38 p. (in German).
4. Seyffarth, P. Atlas of welding TTT diagrams. Düsseldorf: DVS-Verlag, Fachbuchreihe Schweißtechnik 110, 1992. 175 p. (in German).
5. Seyffarth, P.; Scharff, A. Possibilities for calculation of process data and data of weld metal. *Der Praktiker*, No 10. Düsseldorf, 1998, p. 388–393 (in German).
6. Nolde, P.; Meyer, B.; Sarhil, Y. Cold crack safety of the high-strength fine-grained steel S1100QL. *DVS-reports „Welding and cutting“*, No 216, 2001, p. 345–348 (in German).
7. Seyffarth, P.; Kassatkin, O. G. Computed determination of the percentage structural condition in the heat-affected zone of low-alloy steels. *ZIS-Mitteilungen*, No 12. Halle, 1984, p. 1284–1292 (in German).
8. N. N. SYSWELD 2002.1. Paris: ESI Group, 2002.
9. Goldak, J.; McDill, M.; Oddy, A.; House, R.; Chi, X; Bibby, M. Computational heat transfer for weld mechanics. In: *Advances in welding science and technology*, ASM International, 1987, p. 15–20.
10. Pitter, A. Three-dimensional and transient simulation of temperature fields during the WIG-welding of workpieces with temperature dependent material data. Doctor thesis, Clausthal Technical University, 1992. 77 p. (in German).
11. Hamann, R. Numerical calculation of the transient temperature field in the welding body for the wet plasma-MIG-underwater welding process. Düsseldorf, 1996. 134 p. (in German).
12. VDI-Ges. Printed form for calculation of the heat transfer. Berlin: Springer, 2002. CD (in German).
13. Weldable fine-grained structural steels – determination of the cooling time $t_{8/5}$ for identification of welding temperature cycles – Supplement 2. Düsseldorf: Stahleisen, 1993 (in German).
14. Blondeau, R.; Maynier, Ph.; Dollet, J. Forecasting the hardness and resistance of carbon and low-alloy steels according to their structure and composition. *Mem. Sci. Rev. Métallurgie*, No 12, 1973 (in French).
15. Blondeau, R.; Maynier, Ph.; Dollet, J.; Vieillard-Baron, B. Forecasting the hardness, resistance and breaking point of carbon and low-alloy steels according to their composition and heat treatment. *Mem. Sci. Rev. Métallurgie*, No 11, 1975 (in French).